Nanoscale

PAPER

View Article Online
View Journal | View Issue

Cite this: *Nanoscale*, 2022, **14**, 18241

Dehydration does not affect lipid-based hydration lubrication†

Yihui Dong,[a] Nir Kampf,[a] Yaelle Schilt,[b] Wei Cao,[c] Uri Raviv [b] and Jacob Klein *[a]

Received 1st September 2022,
Accepted 22nd November 2022

DOI: 10.1039/d2nr04799c

rsc.li/nanoscale

Phosphatidylcholine (PC) lipid bilayers at surfaces massively reduce sliding friction, *via* the hydration lubrication mechanism acting at their highly-hydrated phosphocholine headgroups, a central paradigm of biological lubrication, particularly at articular cartilage surfaces where low friction is crucial for joint well-being. Nanotribological measurements probed the effect on such lubrication of dehydration by dimethyl sulfoxide (DMSO), known to strongly dehydrate the phosphocholine headgroups of such PC bilayers, *i.e.* reduce the thickness of the inter-bilayer water layer, and thus expected to substantially degrade the hydration lubrication. Remarkably, and unexpectedly, we found that the dehydration has little effect on the friction. We used several approaches, including atomic force microscopy, small- and wide-angle X-ray scattering and all-atom molecular dynamics simulations to elucidate this. Our results show that while DMSO clearly removes hydration water from the lipid head-groups, this is offset by both higher areal head-group density and by rigidity-enhancement of the lipid bilayers, both of which act to reduce frictional dissipation. This sheds strong light on the robustness of lipid-based hydration lubrication in biological systems, despite the ubiquitous presence of bio-osmolytes which compete for hydration water.

Introduction

First described some 2 decades ago, the hydration lubrication mechanism concerns the massive reduction of friction afforded by hydration shells surrounding ions or zwitterions at the slip-plane between sliding surfaces.[1–7] This arises from the tenacious attachment, on a time average, of the hydration layers about the enclosed charges, enabling large loads to be sustained without squeeze-out of the water, while at the same time the rapid exchange of the hydration water ensures the fluidity of the layers, resulting in low frictional dissipation.[1,8] The hydration lubrication paradigm has also illuminated the origins of low friction between biological surfaces sliding past each other under large mechanical stresses. In particular, the very low friction between articular cartilage layers in the major joints (hips and knees), up to physiological pressures of order 10 MPa or more, has been attributed to hydration lubrication between boundary layers comprising phosphatidylcholine (PC) lipid assemblies that expose highly-hydrated lipid head-groups at the slip plane.[9–11] In biological media, including the synovial fluid surrounding joints, there is a significant presence of osmolytes which may compete for hydration water surrounding the lipid headgroups. Indeed, solute additives such as osmolytes and denaturants are well known to regulate the hydration network close to lipid headgroups, affecting the short-range intermembrane repulsive hydration force between them, *e.g.* ref. 12–22. Since the essence of the hydration lubrication mechanism is the low energy dissipation afforded by the tenacious but fluid hydration layers at the slip-plane,[1,8] one expects higher frictional dissipation if the extent of hydration is reduced. The reduced efficiency of hydration lubrication at high salt concentrations, relative to pure water, has been attributed to such an effect,[5] *i.e.* the salt ions compete with the lipid headgroups for the hydration water, reducing the hydration of the latter, though the effect of salt in such a system may be more complicated.[5,6,23]

A crucial question therefore concerns the efficiency of hydration lubrication in environments containing osmolytes

[a]*Department of Molecular Chemistry and Materials Science, Weizmann Institute of Science, Rehovot, 76100, Israel. E-mail: jacob.klein@weizmann.ac.il*
[b]*Institute of Chemistry, The Hebrew University of Jerusalem, Jerusalem 9190401, Israel*
[c]*Department of Physical Chemistry, School of Chemistry, Tel Aviv University, Tel Aviv, 6997801, Israel*

†Electronic supplementary information (ESI) available: S1: zeta potential measurements; S2: AFM imaging of POPC-SUV layers; S3: shear forces between POPC-SUV layers; S4: X-ray scattering measurements on HSPC-SUV dispersions; S5: molecular dynamics simulations; S6: atomic force microscopy (AFM) imaging of HSPC-SUV. Table S1: Zeta potential measurements of HSPC-SUVs, POPC-SUVs; Table S2: Fitting parameters of X-ray scattering measurements on HSPC-SUV; Fig. S1: AFM images of POPC-SUV; Fig. S2: Typical shear force *versus* time traces for the POPC-SUV; Fig. S3: Wide-angle X-ray scattering (WAXS) analysis; Fig. S4: Snapshots of the simulation model of HSPC lipids; Fig. S5: Thickness dependence and order parameter in the simulations; Fig. S6: DMSO number density profile along the normal direction; Fig. S7: Un-normalized radial density function (RDF); Fig. S8: AFM images of HSPC-SUV. See DOI: https://doi.org/10.1039/d2nr04799c

that compete for the hydration water,[13–15,19–22,24] and the purpose of this study is to shed light on this. There are many solutes such as glycerol,[25,26] disaccharide,[27] ethanol,[28] and dimethyl sulfoxide (DMSO)[29] that have been reported to affect the structures of cell membranes through dehydration effects. Among them, DMSO attracted wide attention owing to its amphiphilic character, and its effect on lipid bilayer structure through its competition for water molecules has been frequently studied.[15,30–33] A DMSO molecule can form two hydrogen bonds with water molecules, whose lifetime is about five times longer than hydrogen bonds in bulk water.[34] Thus, DMSO can efficiently compete for water in the vicinity of the lipid surfaces, reduce the extent of hydration, and weaken the repulsive hydration forces between liposomes.[13,15,35,36] These studies[13,15,36] show explicitly that addition of DMSO up to about 10 mol% concentration results in a significant decrease of the inter-bilayer water thickness (a decrease of *ca.* 0.5 ± 0.1 nm). One might therefore expect DMSO to also substantially reduce the hydration lubrication efficiency, as that is predicated on the high hydration reducing frictional energy dissipation on sliding and shear.[6,8,9] More generally, extensive studies have examined in detail the behaviour of water in the vicinity of phospholipid membranes, including the strength of water binding to the carbonyl and phosphate groups of the phosphocholine groups of PC lipids,[37] and the question of dehydration and its effect on the nature of the hydration shell about such headgroups.[38]

Cheng *et al.* studied the effect of DMSO on the structure and interactions of lipid bilayers attached to mica.[14] Below 10 mol% DMSO, they found that DMSO disrupts the water network near the lipid membrane surfaces, and weakens the cohesion within water and the adhesion of water to lipid headgroup.[14] Schrader *et al.* showed that DMSO causes a drastic decrease in the range of the steric hydration repulsion and an increase in adhesion between lipid bilayers.[15] They also found that DMSO enhances the diffusivity of surface water and decreases the range and magnitude of the repulsive forces between the lipid bilayers at less than of <7.5 mol% DMSO.[33]

Here we use DMSO as a canonical dehydrating agent to examine the effect of dehydration on lubrication by boundary layers of PC lipids. Whereas dehydration by DMSO has been shown to weaken hydration repulsion between lipid bilayers,[14,15,33] the effect of dehydration on boundary lubrication between sliding lipid bilayers, central to friction reduction and homeostasis in biomedical and biological systems,[11,39,40] is still unclear. This is because of the essential difference between mechanisms of hydration repulsion, which is an equilibrium effect, and hydration lubrication, which is a dynamic effect concerning energy dissipation on shear. In this study, we use a surface force balance (SFB) to systematically determine the effects of DMSO on the shear and normal forces between surfaces bearing phosphatidylcholine-small unilamellar vesicles (PC-SUVs) or PC bilayers. We then use several approaches including atomic force microscopy (AFM), small- and wide-angle X-ray scattering (SAXS, WAXS) and all-atom molecular dynamics (MD) simulations on the same systems (PC-SUV + DMSO) to provide insight at the molecular level on the effect of the dehydrating molecules on the structure of the lipid layers, and thus on the lubrication mechanism. The DMSO concentration used was less than 10 mol%, because in this range there is no collapse of the lipid headgroup.[14,15] Our results shed light particularly on the different opposing effects of the DMSO on hydration lubrication by the lipid layers, and on the robustness of this mechanism to the presence of dehydrating agents.

Results and discussion

Interactions between lipid-bearing surfaces across water and across DMSO solutions

Normal force profiles. Normal force (F_n) *vs.* surface separation (D) profiles between mica surfaces bearing small unilamellar vesicles of hydrogenated soy phosphatidylcholine (HSPC-SUVs), measured at room temperature (25 °C) using the SFB (Materials and methods), plotted as $F_n(D)/R$ in the Derjaguin approximation (to normalize for slightly different radii of curvature R of the mica sheets), are shown in Fig. 1. The diameter of the vesicles in the dispersion in which the mica surfaces were incubated (Materials and methods) was determined by dynamic light scattering (DLS) as 76.7 ± 0.3 nm (peak value). In the absence of DMSO (Fig. 1(a)), interactions were similar to those seen earlier for the same system:[9] A long-ranged repulsion (D < *ca.* 300 nm) attributed to counterion osmotic pressure due to residual charge on the opposing surfaces (*i.e.* a double-layer electrostatic interaction with a decay length of *ca.* 65 nm), with a sharper rise in F_n onsetting at D < *ca.* 100 nm, likely due to steric repulsion by the opposing surface-attached vesicles (the steric repulsion was somewhat shorter-ranged on second approaches at the same contact points, suggesting, as also previously noted,[9] removal of loosely-attached liposomes on first approach and shear). At the strongest compressions, the surfaces reach a "hard-wall" separation, D_{HW} = 25 ± 2 nm on first approach (filled symbols) and 20 ± 2 nm, on subsequent approaches (empty symbols), corresponding to about 2 lipid bilayers, *i.e.* a flattened layer of HSPC vesicles, on each surface.

Following these measurements, some of the water was replaced by DMSO to reach 3 or 6 mol% DMSO. The resulting $F_n(D)/R$ profiles (Fig. 1(b) and (c) respectively) were broadly similar to those in pure water, save that both the magnitude of the exponentially-decaying long-ranged repulsion as well as the range of the strong steric repulsion was significantly shorter, as seen by the blue-shaded overlay taken from Fig. 1(a), with steric forces commencing at separations $D \lesssim$ 70 nm and $D \lesssim$ 50 nm respectively. We attribute these to the adsorption of DMSO at the outer lipid-bilayer surfaces, acting to reduce the effective surface charge (whose origin is in the negatively-charged underlaying mica surface) responsible for the double-layer repulsion on the one hand, and the adhesion of loosely-attached liposomes on the other. That is, the loosely-attached liposome overlayer becomes even more weakly

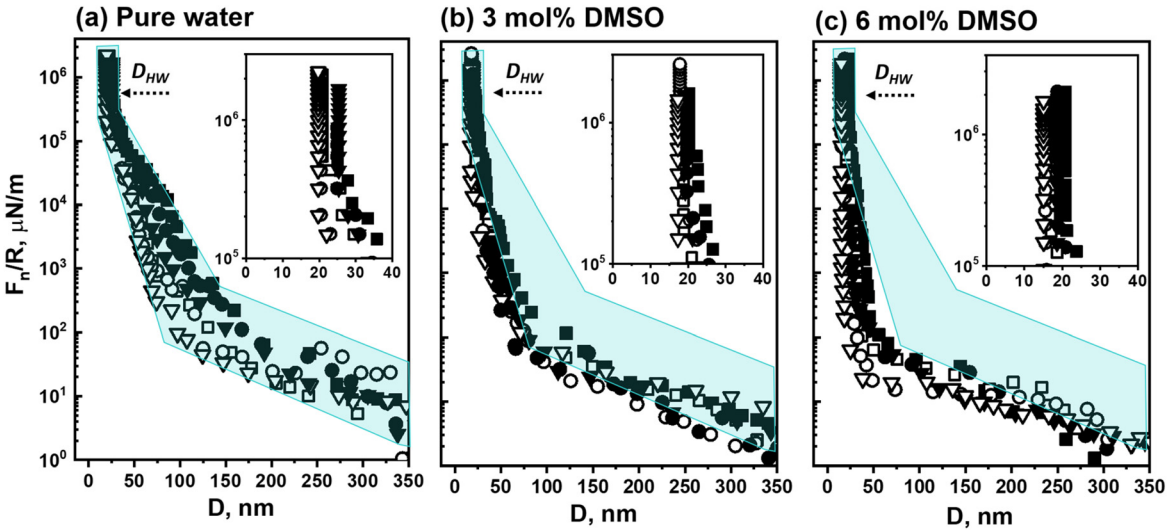

Fig. 1 Normal force (F_n), normalized by the radius of curvature ($R \approx 1$ cm), *versus* surface separation distance (D) between curved mica surfaces (F_n/R *vs.* D), measured for HSPC-SUV coated mica surfaces across pure water (a), 3 mol% DMSO (b), and 6 mol% DMSO (c). The $D = 0$ position is with respect to mica-mica contact in air. The insets show the force–distance profiles close to the hard-wall separations on a magnified scale. For comparison, the blue shaded area represents the range of the force–distance profiles across pure water (a). Filled and empty symbols correspond to first and subsequent approaches.

attached to the outer lipid-bilayer surfaces following addition of the DMSO, which manifests as a weaker steric repulsion. This is supported by zeta-potential measurements (ESI section S1, Table S1†) showing that HSPC-SUVs become more positively charged in DMSO solutions, which would reduce the negative surface potential at the outer surfaces of the mica-attached liposomes. The surface separations D_{HW} at the highest compressions on second approaches were somewhat smaller in the DMSO solutions (in the range (17–20) ± 2 nm) than for the DMSO-free water (20 ± 2 nm). We attribute this in part to dehydration of the bilayers by DMSO, and partly to more efficient removal of the loosely-attached liposomes following the first approach and shear, due to their weaker attachment in the DMSO case as noted above.

Shear (friction) force profiles. Fig. 2 shows typical shear-force ($F_s(t)$) *vs.* time (t) traces at different loads F_n between the HSPC-SUV-bearing mica surfaces across water and across 3 mol% and 6 mol% DMSO solutions, in response to the lateral back-and-forth motion applied to the upper surface. The corresponding F_s *vs.* F_n data is summarized in Fig. 3. The results show that for all 3 systems – DMSO-free water and the 3 mol% and 6 mol% DMSO solutions – the friction remains low and broadly at the same level, with the friction coefficient $\mu = F_s/F_n \approx 10^{-3}$ at the highest loads (at which the corresponding mean contact pressures are of order 100 atm). These μ values are comparable with (if slightly higher than) earlier studies of lubrication by gel-phase PC-SUV boundary layers.[9,10]

Normal and frictional forces between POPC boundary layers. Lipid boundary layers provide hydration lubrication whose efficiency differs considerably between gel-phase lipid assemblies (such as the HSPC-SUV system described above, which is strongly in its gel phase at the room temperature of the measurements) and liquid-phase lipid assemblies.[10,41] To examine the effect of DMSO on the latter we carried out normal and shear force SFB measurements also between layers of palmitoyloleoylphosphatidylcholine small unilamellar vesicles, POPC-SUVs, adsorbed on mica, both across water and across 3 mol% DMSO solution. These have a gel-to-liquid phase main transition temperature $T_m = -2$ °C and so are well in their liquid phase at room temperature. The POPC vesicles diameter in the incubating dispersion was determined (*via* DLS) as 75.8 ± 0.2 nm (peak value). The normal force profiles between mica surface coated with POPC-SUVs across pure water and 3 mol% DMSO are shown in Fig. 4(a), revealing a weak longer ranged double-layer-like repulsion with decay lengths in the range 80 ± 10 nm, and stronger repulsion, attributed to steric interactions of loosely-attached vesicles on each surface, at separations $D \lesssim 100$ nm. The scatter in the range of the different profiles is attributed mostly to differing amounts of loosely adsorbed liposomes on top of the surface-attached layers, which lead to different steric repulsions at different contact points. In contrast to the HSPC-SUV case (Fig. 1), there is only a small difference between the DMSO-free and 3 mol% DMSO profiles for the case of the POPC layers, which may be attributed to little change in the effective surface charge of these layers upon adding the DMSO, as indicated also in its weak effect on the zeta-potential of the POPC-SUVs in dispersion (ESI section S1, Table S1†). Most significantly, the final "hard-wall" separations D_{HW} at the highest compressions in both cases were 8.5 ± 2 and 8.5 ± 0.5 nm in water and DMSO, respectively, indicating a single bilayer of the lipid on each surface, in contrast to the single flattened vesicle layer (*i.e.* two bilayers) on each surface for the case of the gel phase HSPC-SUVs described earlier. This indicates that the POPC

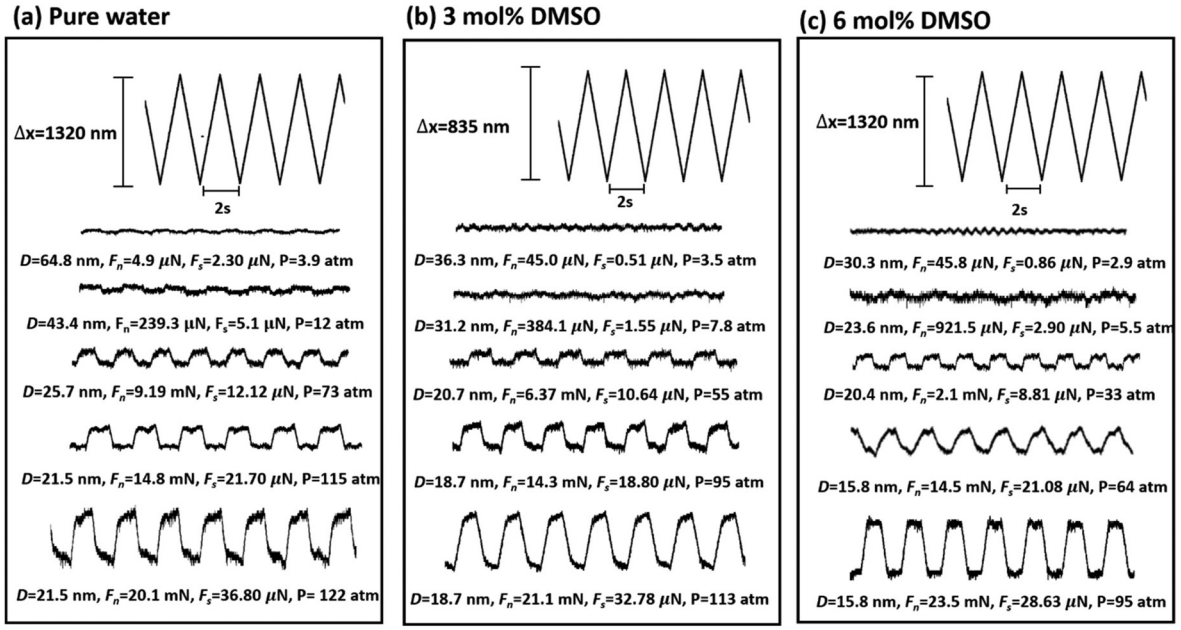

Fig. 2 Typical traces of shear force *versus* time for sliding mica surfaces bearing HSPC-SUV. (a) in pure water; (b) in 3 mol% DMSO; and (c) in 6 mol% DMSO. The uppermost trace in each shows the back-and-forth lateral motion applied to the upper surface, whereas the other traces show the forces transmitted to the lower surface at different loads (F_n), the corresponding separation D, friction forces (F_s), and the mean pressure across the contact region. Each set of traces was recorded during the same approach profile.

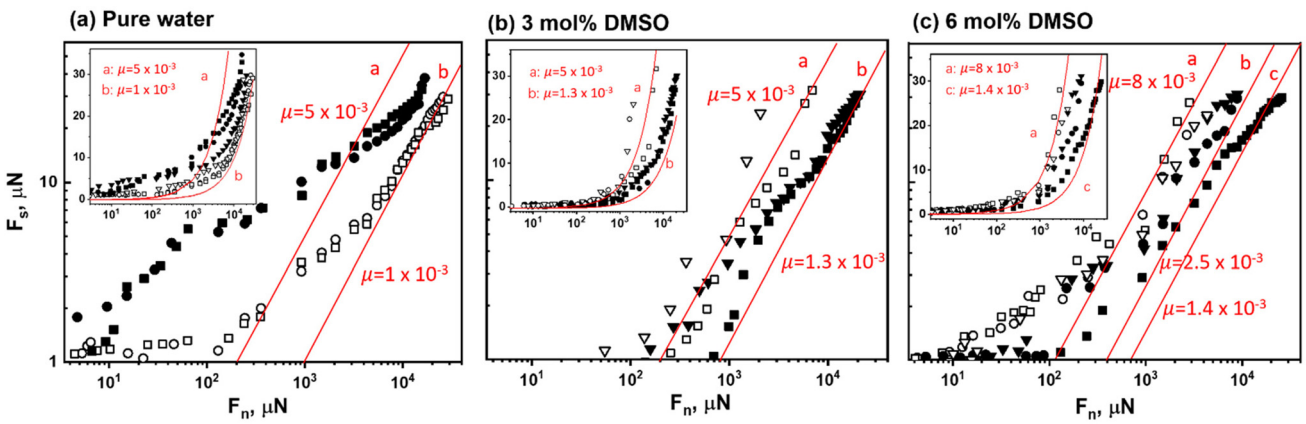

Fig. 3 Shear force as a function of the normal force (F_s *vs.* F_n) between HSPC-SUV-coated mica surface in pure water (a), 3 mol% DMSO (b), and 6 mol% DMSO (c). Red lines in the main (log–log) figure and (lin–log) insets are constant friction coefficients $\mu = F_s/F_n$ enclosing the bulk of the high load data with values as in the adjacent legends. Solid and open symbols represent first and second approaches, respectively.

vesicles ruptured to form bilayers when adsorbed and compressed on the mica substrate, in both water and in 3 mol% DMSO solution, as seen directly *via* AFM measurements (ESI section S2, Fig. S1†), which show them to be flat and continuous, and as also previously reported.[41] We note that in contrast to the HSPC case where D_{HW} (consisting largely of 4 bilayers, 2 on each surface), decreased on subsequent approaches, for the POPC its value – corresponding to 1 bilayer on each surface – changed little between first and subsequent approaches.

Friction force profiles between the POPC layers were determined in the SFB similarly to the HSPC case, and the results, based on shear force traces $F_s(t)$ similar to Fig. 2 (and shown in ESI section S3, Fig. S2†) are summarized in Fig. 4(b). Very low friction forces, not much above the noise level, were recorded between the POPC layers at all applied pressures up to *ca.* 100 atm. Similar results for POPC layers (though across POPC-SUV dispersions rather than pure water) were reported previously.[41] The friction coefficients μ for POPC across pure water and across 3 mol% DMSO solution are both of order 10^{-4} or lower, so that addition of the DMSO is seen to make little difference to the very efficient hydration lubrication in the case boundary layers of this liquid-phase lipid assembly.

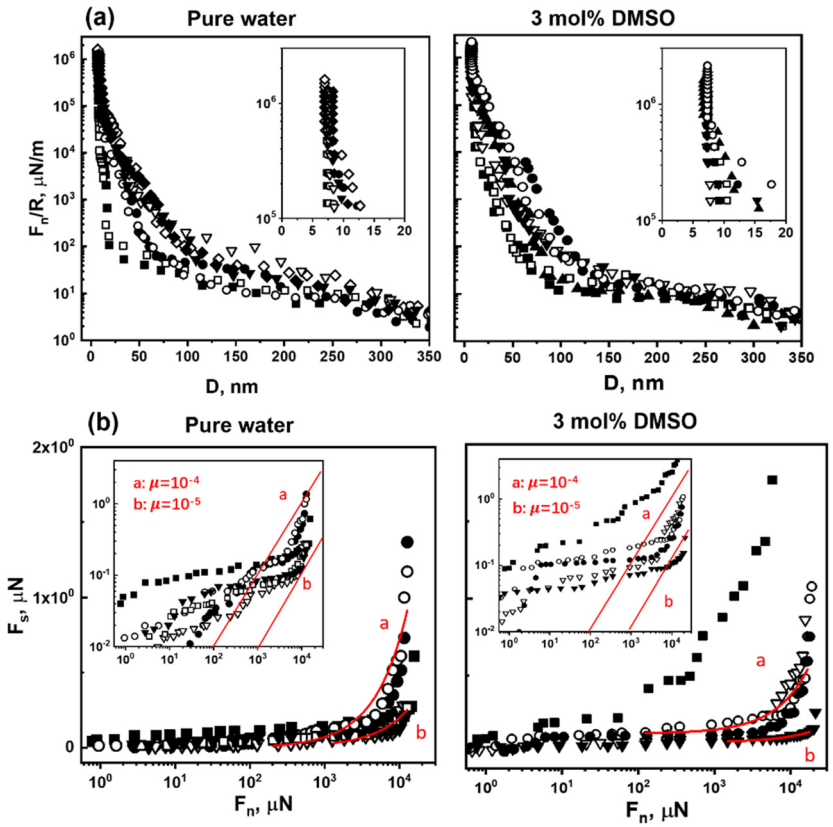

Fig. 4 (a) Normal force (F_n) normalized by the radius of curvature ($R \approx 1$ cm) *versus* surface separation distance (D) between POPC-SUVs coated curved mica surfaces (F_n/R *vs.* D) across pure water and across 3 mol% DMSO. Hard-wall separations are shown at the inset of each figure. (b) Shear force as a function of the normal force (F_s *vs.* F_n) between POPC-SUV coated mica surface across pure water, and 3 mol% DMSO. Red lines are constant friction coefficients $\mu = F_s/F_n$ enclosing the bulk of the high load data with values as in the adjacent legends. Solid and open symbols represent first and second approaches, respectively.

This conclusion is similar to that reached in the case of the gel-phase HSPC lipid boundary layers above. The somewhat superior lubrication by the fluid-phase bilayers (POPC) relative to the gel-phase vesicles (HSPC) is attributed in part to their different structure (bilayers *vs.* liposomes) and in part to their higher level of hydration, and has been considered in detail in ref. 41.

The central new finding of the SFB surface interaction measurements described above, therefore, is that addition of DMSO up to 6 mol% makes little difference to the extremely efficient lubrication by PC lipid surface layers sliding past each other in aqueous media, whether they are in the vesicular (gel-phase HSPC liposomes) or lamellar (liquid-phase POPC bilayers) morphology. This is, on the face of it, a very curious, not to say puzzling observation. This is because such friction reduction, which has been adduced to play a central role in biological and biomedical lubrication,[11,39,40] has been convincingly attributed to the hydration lubrication mechanism at the interface between the highly-hydrated phosphocholine groups exposed at the outer surface of the lipid layers, while DMSO addition to lipids has been demonstrated to disrupt and effectively dehydrate such hydration layers.[14,15,33] To gain insight into why such hydration lubrication by PC layers appears robust to dehydration by the DMSO, it is therefore necessary to examine in more detail the effect of the DMSO on the molecular structure of the lipid bilayers, and how that may affect frictional dissipation as the layers slide past each other. We do this using several approaches: AFM and differential scanning calorimetry (DSC) to examine the changes in the bilayer rigidity; SAXS and WAXS to elucidate the effect of added DMSO on the bilayer characteristics of HSPC-SUVs and MD simulations to examine the effect of added DMSO on HSPC bilayer structure. We should bear in mind however that, with the exception of AFM, these techniques probe properties of unsupported lipid assemblies, in contrast to the mica-attached layers in the SFB studies. We expect the trends indicated for the unsupported bilayers to be valid also for the mica-attached lipid assemblies, as supported by recent studies on increase in lipid thickness for confinement-dehydrated supported bilayers.[42]

SAXS measurements on HSPC-SUV in dispersion

These measurements provide information on the lipid bilayer thickness and, where present, on the lamellar repeat distance within coexisting multilamellar vesicles in the dispersion, as well as on liposome diameters.[13,14,43–46] Fig. 5a shows the

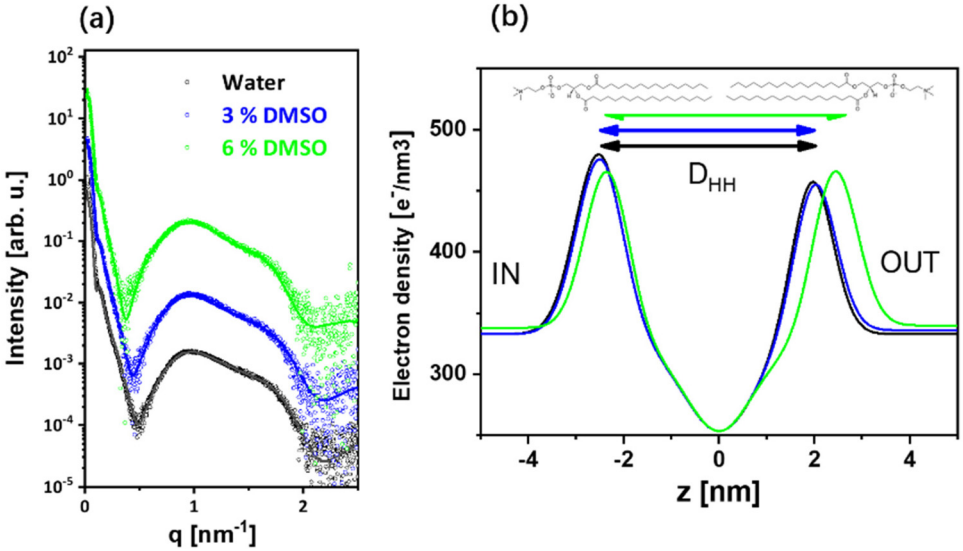

Fig. 5 SAXS analysis of HSPC liposomal dispersions. (a) Azimuthally-averaged, background-subtracted synchrotron SAXS measurements (symbols) from 30 mg mL^{-1} HSPC in aqueous solution of pure water, 3 mol% DMSO, and 6 mol% DMSO. The scattering intensity is plotted as a function of the magnitude of the scattering vector, q. Solid curves correspond to the best-fitted computed scattering curves of the liposomal models (eqn (S2)†). (b) The best fitted electron density profiles of the lipid bilayers along the z-axis, normal to the bilayer plane, used for computing the solid curves in (a). The arrows indicate the bilayer head-to-head distance, D_{HH}, between the opposing lipid phosphate groups. Table S2 (in ESI†) provides the best fitted parameters of the liposomal models.

background-subtracted scattering data (solid symbols) from dispersions of HSPC liposomes at different DMSO concentrations and the models of noninteracting liposomes that best fit the data (solid curves; Materials and methods and ESI section S4†). Fig. 5b shows the corresponding electron density profiles along the radial direction (normal to the bilayer plane) of the best-fitted models, providing the average size of the liposome and the structure of its lipid bilayer (ESI section S4, Table S2†). The radius of the liposome at the middle of the bilayer decreased slightly from 30 ± 1.5 nm to 27 ± 1 nm when DMSO was added (ESI section S4, Table S2†). Adding 3 mol% of DMSO changed the electron density of the medium inside the liposome and the bilayer structure only slightly. The head-to-head distance, D_{HH}, defined from a phosphate group to a phosphate group (the peaks of the electron density profile), increased from 4.47 ± 0.03 nm in water to 4.50 ± 0.03 nm in 3 mol% DMSO. Adding 6 mol% DMSO, however, increased the head-to-head distance significantly to 4.78 ± 0.03 nm and the electron density of the medium inside the liposome to a density equivalent to 4.5 mol% DMSO.[47] In all cases, the bilayers were slightly asymmetric, with a lower density at the outer leaflet. In addition, preliminary wide-angle X-ray scattering (WAXS) measurements on the HSPC-SUV dispersions (ESI section S4C, Fig. S3†) give a clear indication that addition of the DMSO leads to increased areal density of the lipids. This is consistent with the expectation that, for a given volume of the bilayer determined by a constant number of lipids, an increase in its thickness must entail a reduction in the area per lipid headgroup.[48]

In addition, we multiplied the form-factor by two small structure-factor correlation peaks, indicating that the dispersion also contained coexisting multilamellar vesicles. The position of the peaks determined the lamellar repeat distance, D, which decreased from 6.93 nm, in water and 3 mol% DMSO, to 6.77 nm when 6 mol% DMSO was added. This result is consistent with the higher DMSO concentration outside the liposomes, applying osmotic stress to the bilayers.

The main finding of the X-ray scattering measurements is that the bilayer thickness increases upon addition of DMSO, together with increased areal density of the lipids (*i.e.* reduced area/lipid), likely due to reduction of the hydration repulsion between headgroups and consequent stretching of the fatty acid tails due to the van der Waals attraction between them, as seen in earlier studies.[13,30,49]

MD simulations of HSPC bilayers

All-atom MD simulations can provide atomic-level structural and correlational information on the lipid bilayers.[49–51] MD simulations were applied to explore the structure evolution of the lipid bilayer immersed in DMSO solution. HSPC in the gel phase was modeled at room temperature. Initially water and DMSO molecules were randomly added to the two sides of the lipid bilayer, consisting of 200 lipid molecules (100 for each layer). The structure was then relaxed at 300 K and 1 atm. The equilibrium structures were finally collected for further analysis (ESI section S5, Fig. S4†). Fig. 6a shows a snapshot of HSPC with 6 mol% DMSO solution. All simulations were performed by LAMMPS packages[52] (details in Materials and methods and in ESI section S5†). The decrease of the area per lipid and increase of the thickness of the bilayer lipid (D_{HH}), plotted in Fig. 6b, indicate that DMSO is able to tighten the packing efficiency: decrease the area per lipid headgroup and

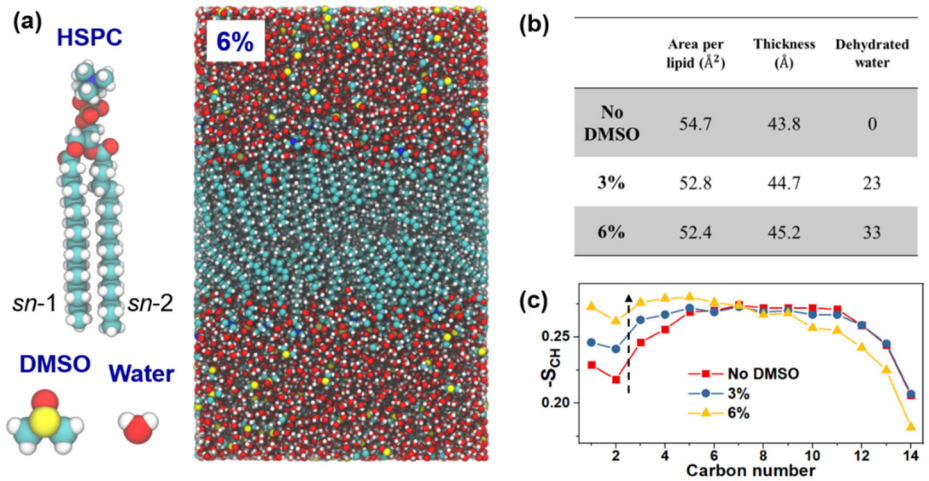

	Area per lipid (Å²)	Thickness (Å)	Dehydrated water
No DMSO	54.7	43.8	0
3%	52.8	44.7	23
6%	52.4	45.2	33

Fig. 6 The simulation results. (a) Atomic models of HSPC, DMSO, and water. Snapshot of the steady-state of HSPC bilayer in a 6 mol% DMSO. The mix of tail lengths in the HSPC was handled by directly building an HSPC lipid. (b) The area per lipid, bilayer thickness (defined by the average vertical distance between phosphorus atoms within two lipid layers), and the number of dehydrated water molecules (defined by the decrease in the number of water molecules within 0.5 nm from each lipid after DMSO was added) as a function of the DMSO concentration. The area per lipid decreases by 3.5% and 4.2%, the thickness increases by 2.1% and 3.2%, and dehydrated water increases by 8.5% and 12.1%, for 3 mol% and 6 mol% DMSO, respectively. (c) The order parameter, $-S_{CH}$, of the phospholipid sn-1 acyl chains (indicated in panel a) of HSPC lipid bilayer for each methylene group (see details of the definition in ESI section S5†).

increase the bilayer thickness. This is the first such simulation of a HSPC lipid bilayer deep in its gel phase: we note especially that the simulated thicker lipid bilayer with DMSO is fully consistent with the SAXS data in Fig. 5. Notably larger concentrations than 6 mol%, which may generate non-monotonic change of the area per lipid,[15] were not studied because the DMSO molecule could penetrate into the lipids.[53] The adsorbed DMSO near the lipid head group can disrupt the hydration network, giving rise to water depletion and enhanced water diffusion.[54] The number of dehydrated water molecules is shown in Fig. 6b. The dehydration can be also seen from the preferential adsorption of DMSO on the lipid head groups (ESI section S5, Fig. S6†) and the un-normalized radial density function of water close to the P and N atoms of the head groups (ESI section S5, Fig. S7†). It is possible that the dehydration results in reduction of the hydration repulsion between the vesicles, partly indicated by the SFB experiments (Fig. 1). The rigidity of the lipid bilayer is characterized by the order parameter,[55] $-S_{CH}$, as shown in Fig. 6c. The increase of $-S_{CH}$ for the methylene groups within the sn-1 chain near the head groups at high DMSO concentration demonstrates the closer packing of the head groups, indicative of larger rigidity. The tightly packed head groups could decrease water hydration by generating steric hinderance.[49] The method to get $-S_{CH}$, and the $-S_{CH}$ of sn-2 chain are explained in the ESI (ESI section S5, Fig. S5b†).

AFM imaging and rigidity measurements

AFM micrographs, Fig. 7 (and ESI section S6, Fig. S8†) reveal a densely-packed array of HSPC-SUVs on the mica (cryo-SEM images,[9,56] show that HSPC-SUVs in fact forms a fully-close-packed array on mica, but some vesicles are detached by the AFM tip during scanning). Additionally, AFM may be used to gauge the local Young's modulus of surface-attached species,

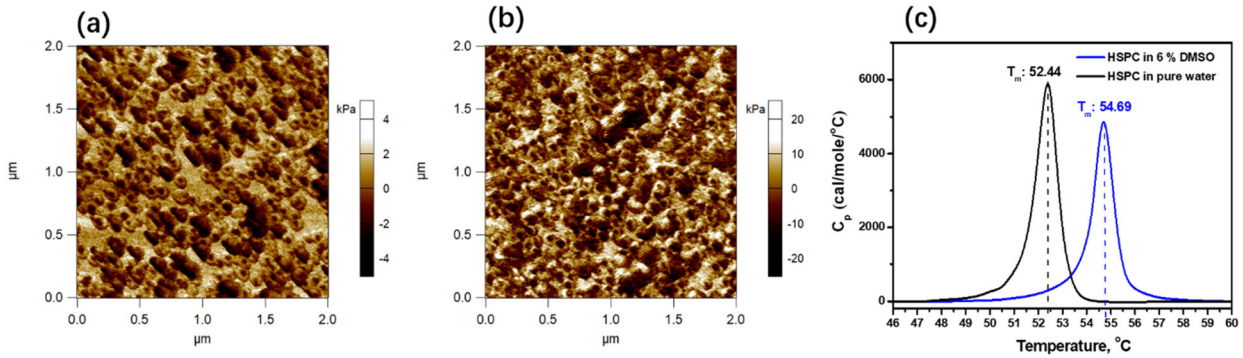

Fig. 7 AFM-measured Young's modulus of HSPC-SUV adsorbed on freshly cleaved mica (a) without and (b) with 6 mol% DMSO solution. (c) DSC measurements of HSPC-SUV dispersion in pure water and in 6 mol% DMSO.

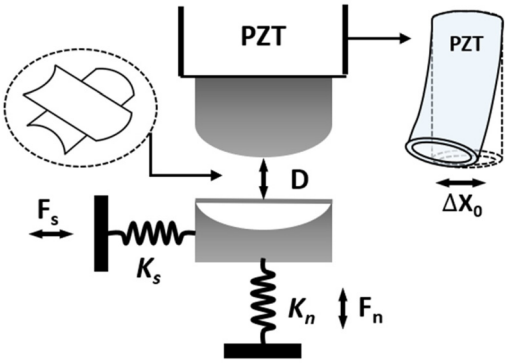

Fig. 8 Schematic illustration of our SFB setup. The two back-silvered mica sheets are glued on two plano-cylindrical quartz lenses and mounted in a crossed-cylinder configuration (shown in the dashed circle), where they may be immersed in the liquid medium. The top lens is mounted on a piezoelectric tube and sideways motion Δx_0 is induced by applying voltages of opposite signs to opposing sectors of the piezoelectric tube. D represents the separation distance between two mica surfaces, K_n and K_s represents the normal and shear spring constants, respectively, and the normal F_n and shear F_s forces are evaluated respectively from the bending of these two orthogonal springs. A more detailed description of the SFB can be found in our earlier publication.[57]

and this is shown in Fig. 7(a) and (b) for HSPC-SUVs adsorbed on mica under DMSO-free water and under 6 mol% DMSO aqueous solution respectively. This technique directly reveals a roughly 5-fold increase in the local Youngs modulus of the vesicles following the DMSO addition, as seen in the respective scales on the right of each micrograph. This increase in the vesicles' rigidity must result from the increase in the bilayer rigidity, and the AFM results thus corroborate through direct measurement the indication of increased bilayer rigidity provided by the increased order parameter in the MD simulation, and by the tighter acyl chain packing indicated by the WAXS (ESI section S4C†).

DSC measurements

The melting temperature (T_m) of HSPC SUVs in water and in 6 mol% DMSO were measured using a DSC (VP-DSC Microcalorimeter), with temperature ranging between 20 and 60 °C and a heating/cooling rate of 0.5 °C min^{-1}. Measurements were performed under N_2 flow. The results are shown in Fig. 7(c): the higher T_m associated with adding 6 mol% DMSO shows the greater stability of the bilayers arising from a tighter acyl-chain packing, again consistent with the X-ray, MD and AFM measurements.

Conclusions

The main new finding of this study is that the extremely efficient lubrication by surface-attached PC lipid bilayers is largely unaffected by addition of DMSO, a molecule known to dehydrate the phosphocholine headgroups exposed by such layers. This is on the face of it very puzzling, insofar as the lubrication by such bilayers is due to the strong reduction in frictional dissipation mediated by the hydration layers on the exposed phosphocholine groups (hydration lubrication),[6,8] so that dehydration should clearly result in increased friction. However, by studying the effect of the DMSO on the lipid bilayers using several different techniques, ranging from small and wide angle X-ray scattering to all-atom MD simulations, we are able to account for this unexpected robustness. Our results reveal that, at the same time as DMSO reduces hydration per headgroup (as described earlier), its presence leads to higher headgroup concentration on the bilayer surface, and moreover renders the bilayer more rigid through stronger acyl chain interactions. Both of these effects are expected to reduce frictional dissipation. The higher lipid areal concentration on adding DMSO offsets the effect of lower hydration level per lipid, while the higher rigidity of the lipid layers reduces viscoelastic frictional dissipation as the opposing layers slide past each other, by reducing local hysteretic deformation. The persistently very good lubrication by the PC lipid layers ($\mu \approx 10^{-3}$) despite their known dehydration by the DMSO indicates that these two effects (higher areal concentration and increased rigidity) mostly compensate the effect on the friction of the loss of hydration. We note that any effects of the DMSO on the interaction between the liposomes and the adsorbing mica substrate is likely to be less important, since the slip occurs entirely at the hydrated lipid–lipid interfaces and is thus less sensitive to details of the lipid-substrate interactions.

This robustness of the friction reduction to dehydration is of clear relevance for biolubrication, which in turn is crucial for the well-being of tissues such as articular cartilage and for associated diseases such as osteoarthritis. This is because the ubiquitous presence of osmolytes (such as urea, glycerol and glycine betaine) in living systems may readily result in dehydration of lipid bilayers[17–21,26] similar to that induced by DMSO in the present study. Thus, our observation of the persistence of low friction provided by lipid bilayers through the hydration lubrication mechanism, despite such dehydration, sheds strong light on nature's ability to maintain efficient hydration lubrication in living systems even in the ubiquitous presence of lipid-dehydrating osmolytes.

Experimental and materials

Materials

Hydrogenated soy phosphatidylcholine (HSPC, 16:0–18:0) and 1-palmitoyl-2-oleoyl-*sn-glycero*-3-phosphocholine (POPC, 16:0–18:1) lipids (purity >99.5%), were purchased from Lipoid GmbH (Ludwigshafen, Germany). DMSO (anhydrous, purity >99.9%) was purchased from Sigma Aldrich. The water used throughout the experiment was highly-purified using a Thermo Scientific Barnstead GenPure water purification system with total organic carbon content ≤1 ppb and resistivity18.2 MΩ.

Preparation of liposomes

The HSPC-SUVs and POPC-SUVs liposomes were prepared using the hydration–extrusion method. The lipids powders

were dispersed in water with an initial concentration of ~6 mM, and then the suspension was sonicated in a water bath sonicator for 15 min (~65 °C for HSPC and room temperature for POPC) and with vortexing for 5 min, to obtain a homogeneous dispersion of multilamellar vesicles (MLVs). Then the MLVs were downsized to form small unilamellar vesicles (SUVs) through extruding the MLV dispersion through polycarbonate membranes with pore sizes of ~400, 100, and 50 nm for 5, 10, and 12 times, respectively, using the extruder chamber with the temperature higher than the T_m of each lipid which was controlled by a water circulation bath.

Surface force balance (SFB) measurements

The SFB setup and the detailed procedures for the measurements have been described previously refs; a schematic of shown in Fig. 8.

Briefly, two cleaved molecularly-smooth mica sheets were back-silvered and mounted in the SFB in a crossed-cylinder orientation as indicated (Fig. 8). The closest separation between them (D) was measured *via* interference fringes of equal chromatic order (FECO) (accuracy ±2–3 Å), and normal (F_n) and shear (F_s) forces between them measured *via* bending of the respective springs K_n and K_s (Fig. 8).

The liposomes-coated mica surfaces were prepared as follows: the freshly cleaved mica facets glued on their lenses were immersed in a 0.3 mM liposome dispersion (either HSPC-SUV or POPC-SUV), prepared with purified conductivity water at room temperature, for overnight incubation. After the incubation, they were washed with pure water and then mounted in the SFB. Diameters of the contact area depend on compression but are typically in the range 10–30 μm as seen from the optical fringe shape,[57] and do not vary significantly between first and subsequent approaches. Following measurements across pure water, some water was replaced by concentrated DMSO solution to achieve the concentration of the DMSO–water to 3 mol% and 6 mol%, respectively, and allowed to equilibrate for between 2 h and overnight (no systematic differences were seen for different equilibration times). Since the typical contact areas (lateral dimensions O (10 μm) over which forces are measured are much smaller than the area (lateral dimensions O (mm)) of the mica, each new area of contact between the surfaces involves essentially pristine surfaces and is unaffected by measurements at previous contact points.

X-ray scattering measurements

We performed solution small-angle X-ray scattering (SAXS) measurements on the liposome dispersions and controls at ID02 synchrotron beamline at the ESRF.[58] The sample-to-detector distance was 2.5 m, and the X-ray wavelength was 0.0995 nm. We manually injected 100 μL of each sample into a 2 mm thick quartz capillary flow cell. 30 frames were measured while the sample was flowing through the capillary. The exposure time was 50 ms per frame. As a reference, we also measured the solvent of each sample. Scattering data were recorded on a 2D Eiger2 4M (Dectris AG) detector, azimuthally averaged,[59] and the scattering intensity was plotted as a function of the magnitude of the scattering vector, q. The scattering curve of solvent was subtracted from the scattering curve of the sample and analyzed using X+ program.[60]

The scattering amplitude of non-interacting liposomes in dilute solution is the Fourier transform of their electron density contrast from the solvent. We modeled the electron density contrast of the lipid bilayer as five spherical shells with Gaussian electron density profiles along the radial direction. In addition, we modeled the inner medium of the liposome as a uniform spherical shell, with an electron density that could differ from the solvent outside the liposomes (ESI, eqn (S1)†). To account for the size distribution of liposomes, the radius of the uniform sphere followed a Gaussian distribution function. The solution scattering intensity of the noninteracting liposomes, known as the form-factor, is the square of the scattering amplitude, averaged over all the orientations (ESI section 2†). Further details about this model are provided in our earlier publication and in the ESI section 2.†[61] We also included small structure factor correlation peaks with Gaussian line shapes, corresponding to a small fraction of coexisting liposomes with more than one bilayer. Wide angle X-ray scattering measurements were also carried out, and are detailed in the ESI section 2C.†

Molecular dynamic (MD) simulations

Simulation models and methods. The initial lipid bilayer was built from 100 × 2 HSPC lipids with 100 in each leaflet. To model its gel phase, lipids were initially titled manually to 15° with respect to the normal direction. Such initial structure was reported to successfully predict the gel phase of lipid bilayers.[62] Water molecules were added to the top of the lipid surfaces from both sides. The number of water molecules was 10 000 for system without DMSO. The number of DMSO was set according to the concentration studied in the experiments, *i.e.*, 300 for 3 mol% and 600 for 6 mol%. The total solvent molecules were fixed to 10 000. All the inter- and intra-molecular interactions were performed by the all-atom CHARMM36 force field.[63,64] The short-range van der Waals were computed with a cutoff distance of 1.0 nm and long-range electrostatic interactions were calculated with the particle–particle–particle–mesh (PPPM) method.[65] Periodic boundary condition was applied to all the three directions. The initial structure was first minimized, and then equilibrated at temperature of 298 K and pressure of 1 atom for 2 ns at a timestep of 1 fs. Another 2 ns equilibrium run was performed and the trajectories were collected for further analysis.

The snapshots of the initial and the relaxed structure without DMSO are shown in Fig. S3.† For simulations with only water and lipid bilayer, the area per lipid is calculated to be 54.7 Å^2, which is a bit larger than its fluid phase,[66] 49.6 Å^2. The head to head distance (defined by the distance between phosphorus atoms) in the simulations was analyzed to show the equilibrium of the simulation systems, see Fig. S4a.†

Order parameter of the lipid bilayer. The order parameter $-S_{CH}$ was calculated to analyze to orderliness of the acyl

chains in lipids, defined as

$$S_{CH} = \langle 3\cos^2\theta - 1\rangle/2$$

where θ is the angle between the C–H bond vector and the bilayer normal. It describes the orientation of the C–H bond vector within the methylene groups and the normal direction of the lipid bilayer, which is set to be the vertical direction in the simulation model. The angular brackets stand for the molecular and ensemble average. The profile of the sn-2 acyl chain is plotted in Fig. S4b.†

Author contributions

YD designed and carried out experiments and wrote the paper; NK carried out experiments and contributed to writing the paper; YS and UR carried out the X-ray scattering experiments and contributed to writing the paper; WC carried out MD calculations and contributed to writing the paper; JK conceived the project and wrote the paper.

Conflicts of interest

There are no conflicts to declare.

Acknowledgements

We appreciate a useful comment by Ran Tivony. We thank the European Research Council (advanced grant CartiLube 743016), the McCutchen Foundation, the Israel Science Foundation – National Natural Science Foundation of China joint research program (grant 3618/21), the Israel Ministry of Science and Technology (grant 3-15716), and the Israel Science Foundation (grant 1229/20) for financial support. This work was made possible partly through the historic generosity of the Perlman family.

References

1 U. Raviv and J. Klein, Fluidity of Bound Hydration Layers, *Science*, 2002, **297**(5586), 1540–1543.
2 U. Raviv, S. Giasson, N. Kampf, J.-F. Gohy, R. Jérôme and J. Klein, Lubrication by charged polymers, *Nature*, 2003, **425**(6954), 163–165.
3 T. Murakami, S. Yarimitsu, K. Nakashima, Y. Sawae and N. Sakai, Influence of synovia constituents on tribological behaviors of articular cartilage, *Friction*, 2013, **1**(2), 150–162.
4 P. Hilšer, A. Suchánková, K. Mendová, K. E. Filipič, M. Daniel and M. Vrbka, A new insight into more effective viscosupplementation based on the synergy of hyaluronic acid and phospholipids for cartilage friction reduction, *Biotribology*, 2021, **25**, 100166.
5 M. Chen, W. H. Briscoe, S. P. Armes and J. Klein, Lubrication at Physiological Pressures by Polyzwitterionic Brushes, *Science*, 2009, **323**(5922), 1698–1701.
6 L. Ma, A. Gaisinskaya-Kipnis, N. Kampf and J. Klein, Origins of hydration lubrication, *Nat. Commun.*, 2015, **6**(1), 6060.
7 W. H. Briscoe, S. Titmuss, F. Tiberg, R. K. Thomas, D. J. McGillivray and J. Klein, Boundary lubrication under water, *Nature*, 2006, **444**(7116), 191–194.
8 J. Klein, Hydration lubrication, *Friction*, 2013, **1**(1), 1–23.
9 R. Goldberg, *et al.*, Boundary Lubricants with Exceptionally Low Friction Coefficients Based on 2D Close-Packed Phosphatidylcholine Liposomes, *Adv. Mater.*, 2011, **23**(31), 3517–3521.
10 R. Sorkin, *et al.*, Origins of extreme boundary lubrication by phosphatidylcholine liposomes, *Biomaterials*, 2013, **34**(22), 5465–5475.
11 S. Jahn, J. Seror and J. Klein, Lubrication of Articular Cartilage, *Annu. Rev. Biomed. Eng.*, 2016, **18**(1), 235–258.
12 L. I. Viera, S. Alonso-Romanowski, V. Borovyagin, M. R. Feliz and E. A. Disalvo, Properties of gel phase lipid-trehalose bilayers upon rehydration, *Biochim. Biophys. Acta*, 1993, **1145**(1), 157–167.
13 M. A. Kiselev, P. Lesieur, A. M. Kisselev, C. Grabielle-Madelmond and M. Ollivon, DMSO-induced dehydration of DPPC membranes studied by X-ray diffraction, small-angle neutron scattering, and calorimetry, *J. Alloys Compd.*, 1999, **286**(1), 195–202.
14 C. Y. Cheng, J. Song, J. Pas, L. H. Meijer and S. Han, DMSO induces dehydration near lipid membrane surfaces, *Biophys. J.*, 2015, **109**(2), 330–339.
15 A. M. Schrader, S. H. Donaldson, J. Song, C.-Y. Cheng, D. W. Lee, S. Han and J. N. Israelachvili, Correlating steric hydration forces with water dynamics through surface force and diffusion NMR measurements in a lipid–DMSO–H_2O system, *Proc. Natl. Acad. Sci. U. S. A.*, 2015, **112**(34), 10708–10713.
16 A. Wolde-Kidan, Q. D. Pham, A. Schlaich, P. Loche, E. Sparr, R. R. Netz and E. Schneck, Influence of polar co-solutes and salt on the hydration of lipid membranes, *Phys. Chem. Chem. Phys.*, 2019, **21**(31), 16989–17000.
17 A. Maiti and S. Daschakraborty, How Do Urea and Trimethylamine N-Oxide Influence the Dehydration-Induced Phase Transition of a Lipid Membrane?, *J. Phys. Chem. B*, 2021, **125**(36), 10149–10165.
18 Z. Xia and B. L. Lau, Mitigating effects of osmolytes on the interactions between nanoparticles and supported lipid bilayer, *J. Colloid Interface Sci.*, 2020, **568**, 1–7.
19 A. Maiti and S. Daschakraborty, Can Urea and Trimethylamine-N-oxide Prevent the Pressure-Induced Phase Transition of Lipid Membrane?, *J. Phys. Chem. B*, 2022, **126**(7), 1426–1440.
20 E. J. Guinn, L. M. Pegram, M. W. Capp, M. N. Pollock and M. T. Record, Quantifying why urea is a protein denaturant, whereas glycine betaine is a protein stabilizer, *Proc. Natl. Acad. Sci. U. S. A.*, 2011, **108**(41), 16932–16937.

21 N. Kumar and N. Kishore, Synergistic behavior of glycine betaine-urea mixture: a molecular dynamics study, *J. Chem. Phys.*, 2013, **139**(11), 115104.
22 Q. D. Pham, A. Wolde-Kidan, A. Gupta, A. Schlaich, E. Schneck, R. R. Netz and E. Sparr, Effects of Urea and TMAO on Lipid Self-Assembly under Osmotic Stress Conditions, *J. Phys. Chem. B*, 2018, **122**(25), 6471–6482.
23 R. Goldberg, A. Schroeder, Y. Barenholz and J. Klein, Interactions between Adsorbed Hydrogenated Soy Phosphatidylcholine (HSPC) Vesicles at Physiologically High Pressures and Salt Concentrations, *Biophys. J.*, 2011, **100**(10), 2403–2411.
24 S. Kundu, S. Malik, M. Ghosh, S. Nandi, A. Pyne, A. Debnath and N. Sarkar, A Comparative Study on DMSO-Induced Modulation of the Structural and Dynamical Properties of Model Bilayer Membranes, *Langmuir*, 2021, **37**(6), 2065–2078.
25 J. E. Lovelock, The mechanism of the protective action of glycerol against haemolysis by freezing and thawing, *Biochim. Biophys. Acta*, 1953, **11**(1), 28–36.
26 E. B. de Sousa, G. C. Dos Santos Junior, R. P. Aguiar, R. da Costa Sartore, A. C. L. de Oliveira, F. C. L. Almeida, V. M. Neto and D. P. Aguiar, Osteoarthritic Synovial Fluid Modulates Cell Phenotype and Metabolic Behavior In Vitro, *Stem Cells Int.*, 2019, **2019**, 8169172.
27 B. Kent, T. Haußß, B. Demé, V. Cristiglio, T. Darwish, T. Hunt, G. Bryant and C. J. Garvey, Direct Comparison of Disaccharide Interaction with Lipid Membranes at Reduced Hydrations, *Langmuir*, 2015, **31**(33), 9134–9141.
28 M. Patra, E. Salonen, E. Terama, I. Vattulainen, R. Faller, B. W. Lee, J. Holopainen and M. Karttunen, Under the Influence of Alcohol: The Effect of Ethanol and Methanol on Lipid Bilayers, *Biophys. J.*, 2006, **90**(4), 1121–1135.
29 J. E. Lovelock and M. W. H. Bishop, Prevention of Freezing Damage to Living Cells by Dimethyl Sulphoxide, *Nature*, 1959, **183**(4672), 1394–1395.
30 Z. W. Yu and P. J. Quinn, Phase stability of phosphatidylcholines in dimethylsulfoxide solutions, *Biophys. J.*, 1995, **69**(4), 1456–1463.
31 A. A. Gurtovenko and J. Anwar, Modulating the structure and properties of cell membranes: the molecular mechanism of action of dimethyl sulfoxide, *J. Phys. Chem. B*, 2007, **111**(35), 10453–10460.
32 R. Notman, M. Noro, B. O'Malley and J. Anwar, Molecular basis for dimethylsulfoxide (DMSO) action on lipid membranes, *J. Am. Chem. Soc.*, 2006, **128**(43), 13982–13983.
33 A. M. Schrader, C.-Y. Cheng, J. N. Israelachvili and S. Han, Communication: Contrasting effects of glycerol and DMSO on lipid membrane surface hydration dynamics and forces, *J. Chem. Phys.*, 2016, **145**(4), 041101.
34 A. Luzar and D. Chandler, Structure and hydrogen bond dynamics of water–dimethyl sulfoxide mixtures by computer simulations, *J. Chem. Phys.*, 1993, **98**(10), 8160–8173.
35 A. Schlaich, J. Kappler and R. Netz, Hydration Friction in Nanoconfinement: From Bulk via Interfacial to Dry Friction, *Nano Lett.*, 2017, **17**, 5969–5979.
36 V. I. Gordeliy, M. A. Kiselev, P. Lesieur, A. V. Pole and J. Teixeira, Lipid Membrane Structure and Interactions in Dimethyl Sulfoxide/Water Mixtures, *Biophys. J.*, 1998, **75**(5), 2343–2351.
37 F. Martelli, J. Crain and G. Franzese, Network Topology in Water Nanoconfined between Phospholipid Membranes, *ACS Nano*, 2020, **14**, 8616–8623.
38 M. Chattopadhyay, E. Krok, H. Orlikowska, P. Schwille, H. Franquelim and L. Piatkowski, Hydration Layer of Only a Few Molecules Controls Lipid Mobility in Biomimetic Membranes, *J. Am. Chem. Soc.*, 2021, **143**, 14551–14562.
39 W. Lin and J. Klein, Recent Progress in Cartilage Lubrication, *Adv. Mater.*, 2021, **33**(18), 2005513.
40 W. Lin and J. Klein, Hydration Lubrication in Biomedical Applications: From Cartilage to Hydrogels, *Acc. Chem. Res.*, 2022, **3**(2), 213–223.
41 R. Sorkin, N. Kampf, L. Zhu and J. Klein, Hydration lubrication and shear-induced self-healing of lipid bilayer boundary lubricants in phosphatidylcholine dispersions, *Soft Matter*, 2016, **12**(10), 2773–2784.
42 L. Mears, S. Abbott, R. Barker, W. de Vos, S. Prescott and R. Richardson, Structural Evidence for a Reinforcing Response and Retention of Hydration During Confinement of Cartilage Lipids, *Front. Phys.*, 2021, **9**, 703472.
43 S. Tristram-Nagle, T. Moore, H. I. Petrache and J. F. Nagle, DMSO produces a new subgel phase in DPPC: DSC and X-ray diffraction study, *Biochim. Biophys. Acta*, 1998, **1369**(1), 19–33.
44 L. Fink, C. Allolio, J. Feitelson, C. Tamburu, D. Harries and U. Raviv, Bridges of Calcium Bicarbonate Tightly Couple Dipolar Lipid Membranes, *Langmuir*, 2020, **36**(36), 10715–10724.
45 P. V. Konarev, A. Y. Gruzinov, H. D. Mertens and D. I. Svergun, Restoring structural parameters of lipid mixtures from small-angle X-ray scattering data, *J. Appl. Crystallogr.*, 2021, **54**(1), 169–179.
46 Y. Schilt, T. Berman, X. Wei, Y. Barenholz and U. Raviv, Using solution X-ray scattering to determine the high-resolution structure and morphology of PEGylated liposomal doxorubicin nanodrugs, *Biochim. Biophys. Acta, Gen. Subj.*, 2016, **1860**(1, Part A), 108–119.
47 J. M. G. Cowie and P. M. Toporowski, Association in the Binary Liquid System Dimethyl Sulphoxide-Water, *Can. J. Chem.*, 1961, **39**(11), 2240–2243.
48 P. Szekely, T. Dvir, R. Asor, R. Resh, A. Steiner, O. Szekely, A. Ginsburg, J. Mosenkis, V. Guralnick, Y. Dan, T. Wolf, C. Tamburu and U. Raviv, Effect of Temperature on the Structure of Charged Membranes, *J. Phys. Chem. B*, 2011, **115**(49), 14501–14506.
49 R. K. Venkatraman and C. R. Baiz, Ultrafast Dynamics at the Lipid–Water Interface: DMSO Modulates H-Bond Lifetimes, *Langmuir*, 2020, **36**(23), 6502–6511.
50 E. Lee, A. Kundu, J. Jeon and M. Cho, Water hydrogen-bonding structure and dynamics near lipid multibilayer surface: Molecular dynamics simulation study with direct

experimental comparison, *J. Chem. Phys.*, 2019, **151**(11), 114705.

51 Y. Nagata and S. Mukamel, Vibrational Sum-Frequency Generation Spectroscopy at the Water/Lipid Interface: Molecular Dynamics Simulation Study, *J. Am. Chem. Soc.*, 2010, **132**(18), 6434–6442.

52 S. Plimpton, Fast Parallel Algorithms for Short-Range Molecular Dynamics, *J. Comput. Phys.*, 1995, **117**(1), 1–19.

53 J. Lin, B. Novak and D. Moldovan, Molecular Dynamics Simulation Study of the Effect of DMSO on Structural and Permeation Properties of DMPC Lipid Bilayers, *J. Phys. Chem. B*, 2012, **116**(4), 1299–1308.

54 C.-Y. Cheng, J. Song, J. Pas, L. H. H. Meijer and S. Han, DMSO Induces Dehydration near Lipid Membrane Surfaces, *Biophys. J.*, 2015, **109**(2), 330–339.

55 T. J. Piggot, J. R. Allison, R. B. Sessions and J. W. Essex, On the Calculation of Acyl Chain Order Parameters from Lipid Simulations, *J. Chem. Theory Comput.*, 2017, **13**(11), 5683–5696.

56 J. Seror, L. Zhu, R. Goldberg, A. J. Day and J. Klein, Supramolecular synergy in the boundary lubrication of synovial joints, *Nat. Commun.*, 2015, **6**(1), 6497.

57 J. Klein and E. Kumacheva, Simple liquids confined to molecularly thin layers. I. Confinement-induced liquid-to-solid phase transitions, *J. Chem. Phys.*, 1998, **108**(16), 6996–7009.

58 T. Narayanan, M. Sztucki, T. Zinn, J. Kieffer, A. Homs-Puron, J. Gorini, P. Van Vaerenbergh and P. Boesecke, Performance of the time-resolved ultra-small-angle X-ray scattering beamline with the Extremely Brilliant Source, *J. Appl. Crystallogr.*, 2022, **55**(1), 98–111.

59 M. Sztucki, *SAXSutilities: a graphical user interface for processing and analysis of Small-Angle X-ray Scattering data*, Zenodo, 2021.

60 T. Ben-Nun, A. Ginsburg, P. Szekely and U. Raviv, X plus : a comprehensive computationally accelerated structure analysis tool for solution X-ray scattering from supramolecular self-assemblies, *J. Appl. Crystallogr.*, 2010, **43**, 1522–1531.

61 Y. Schilt, T. Berman, X. Wei, Y. Barenholz and U. Raviv, Using solution X-ray scattering to determine the high-resolution structure and morphology of PEGylated liposomal doxorubicin nanodrugs, *Biochim. Biophys. Acta, Gen. Subj.*, 2016, **1860**(1), 108–119.

62 A. Yang, T. C. Moore, C. R. Iacovella, M. Thompson, D. J. Moore and C. McCabe, Examining Tail and Headgroup Effects on Binary and Ternary Gel-Phase Lipid Bilayer Structure, *J. Phys. Chem. B*, 2020, **124**(15), 3043–3053.

63 J. B. Klauda, R. M. Venable, J. A. Freites, J. W. O'Connor, D. J. Tobias, C. Mondragon-Ramirez, I. Vorobyov, A. D. MacKerell and R. W. Pastor, Update of the CHARMM All-Atom Additive Force Field for Lipids: Validation on Six Lipid Types, *J. Phys. Chem. B*, 2010, **114**(23), 7830–7843.

64 W. Yu, X. He, K. Vanommeslaeghe and A. D. MacKerell Jr., Extension of the CHARMM general force field to sulfonyl-containing compounds and its utility in biomolecular simulations, *J. Comput. Chem.*, 2012, **33**(31), 2451–2468.

65 E. L. Pollock and J. Glosli, Comments on P3M, FMM, and the Ewald method for large periodic Coulombic systems, *Comput. Phys. Commun.*, 1996, **95**(2), 93–110.

66 D. Drabik, G. Chodaczek, S. Kraszewski and M. Langner, Mechanical Properties Determination of DMPC, DPPC, DSPC, HSPC Solid-Ordered Bilayers, *Langmuir*, 2020, **36**(14), 3826–3835.